SURGICAL CRS STACKING

J. H. Faccipieri, D. Rueda, T. A. Coimbra, I. L. Rodrigues, A. L. Farias, and M. Tygel

email: *jorge.faccipieri@gmail.com, drs6120@gmail.com, tgo.coimbra@gmail.com, ian.liu88@gmail.com, armandolfarias@gmail.com and tygel@ime.unicamp.br*
keywords: *Common Reflection Surface (CRS), Estimation strategy*

ABSTRACT

Seismic processing techniques that are based on multi-parametric traveltimes, albeit providing good imaging and inversion results, carry the burden of much intensive and costly computation effort. That is the case of the multifocusing (MF) and Common-Reflection-Surface (CRS) methods, for which a significant part of the literature is devoted to strategies and algorithms so that various parameters are estimated in an optimal way. In the case of CRS, the traveltimes depend on three and eight parameters in the 2D and 3D situations, respectively. Moreover, the parameter estimation is supposed to be computed at each sample of the zero-offset (ZO) stacked section or volume. In many real-data cases the computational costs are unfeasible. In this work, we propose a so-called Surgical CRS, which consists of the following steps (a) User-selection at a few (picked) points, on an initial (given) CMP stacked section and global exhaustive evaluation of CRS parameters on these points; (b) Interpolation/extrapolation of the obtained CRS parameters to fill out all sample positions that comprise the ZO section or volume to be constructed; (c) Global refinement of CRS parameters using the previously obtained parameter as initial values; (d) Computation of the CRS stack with the refined parameters and finally (e) This process is repeated by adding, subtracting or editing points until a desired result is achieved. The results obtained with this approach were able to produce better stacked sections and reduce its the computational cost.

INTRODUCTION

Seismic processing, as a rule, consists of a sequence of well-defined steps, in which each of them influences the next. As a consequence, it is natural that each step is carefully controlled, many times with the help of an interpreter. Because of the involved time and costs, a great appeal exists in so-called data-driven procedures that exclude or at least minimize human interference. Best examples in this direction are imaging techniques based on multi-parametric traveltime moveouts, such as the Common-Reflection-Surface (CRS) (e.g., Müller et al., 1997; Jäger et al., 2001; Bergler et al., 2002; Garabito et al., 2001; Duveneck, 2004; Spinner and Mann, 2005; Hertweck et al., 2007; Dell and Vanelle, 2012; Faccipieri et al., 2013; Garabito et al., 2013; Dell et al., 2014; Gelius and Tygel, 2015) and the Multifocus (MF) (e.g., Gelchinsky et al., 1999a,b; Landa et al., 1999; Berkovitch et al., 2008; Landa et al., 2010) methods. At the same time, new multi-parametric moveouts have been also introduced (e.g., Fomel and Kazinnik, 2013; Schwarz et al., 2014) and their application is starting to be be explored (see, e.g., Perroud et al., 2014).

In the following, we focus on the CRS method, and introduce a new CRS workflow, referred to as *Surgical CRS*. As explained below, this workflow is an iterative and interactive process: At each iteration, full estimation of CRS parameters is restricted to a few, carefully (or "surgically ") chosen sample points only. Away from these sample points, the corresponding CRS parameter values are obtained by interpolation or extrapolation procedures.

The CRS parameter values defined at all samples of the output volume to be constructed, constitute initial values (or guides). For each CRS parameter, the corresponding guide can be roughly interpreted as a low-frequency trend of that parameter. With the help of the guides as initial values and also small deviation windows allowed, global refinement of CRS parameters is performed and a CRS stacked obtained.

The interactive part of the process lies on how, in each iteration, the few "surgical"points are selected by manual picking. This is done as follows: In the first step, those points are chosen along clearly defined events on a conventional common-midpoint (CMP) stacked section or volume, supposedly given. At each subsequent step, the surgical points are chosen from CRS-stacked volumes obtained in the previous iteration. This process is repeated (adding, subtracting or editing points) until the desired result is achieved.

The main advantage of the proposed workflow is the significative reduction of full parameter estimations, upon them to fewer points of higher interpretative value. A possible drawback is the dependence of manual picks in the selection of those points.

The surgical CRS has been applied to a 2D real land dataset. The obtained results were superior in comparison with the conventional techniques (CMP stacking and fully data-driven CRS stacking). The intervention of an interpreter/user to guide the estimation intervals of CRS parameters (locally) was fundamental to achieve these results. Due to the geological content incorporated in the CRS estimation, several artifacts (e.g., so-called CRS worms) have been eliminated. As expected, the processing time required to perform a CRS estimation and stacking was significantly reduced. Besides the above abstract and introduction, the present work comprises the following sections: Brief description of the traveltime operator used in CRS; Detailed, step-by-step explanation of the surgical CRS workflow; Application of the surgical CRS to a real-data example, together with discussion and comparison to available data-driven counterparts. Conclusions, Acknowledgments and References complete the work.

CRS OPERATOR

The CRS operator represents the traveltime of primary, non-converted, reflection response of an unknown depth reflector due source-receiver pairs arbitrarily located in the vicinity of a reference (central) point. In the 2D situation of a horizontal seismic acquisition line envisaged here, the source-receiver pairs are specified by (scalar) midpoint and half-offset coordinates (m, h). The central point is specified by the coordinates $m = m_0$ and $h = 0$. Under these conditions, the CRS traveltime represents the moveout for reflections in the vicinity of a (central) zero-offset (ZO) defined by the central point, m_0. The 2D CRS operator represents a simple Taylor polynomial of quadratic traveltime (e.g., Jäger et al., 2001),

$$t_{CRS}^2(m,h) = [t_0 + a\Delta m]^2 + B\Delta m^2 + Ch^2 \,, \tag{1}$$

in which $\Delta m = m - m_0$ is midpoint displacement with respect to m_0 and

$$a = \frac{\partial t_{CRS}}{\partial m}, \quad B = \frac{\partial^2 t_{CRS}}{\partial m^2} \quad \text{and} \quad C = \frac{\partial^2 t_{CRS}}{\partial h^2} \,, \tag{2}$$

all derivatives evaluated at $m = m_0$ and $h = 0$. It is to be noted that the absence of the linear derivative with respect to h ($\partial t_{CRS}/\partial h = 0$) is a consequence of the source-receiver reciprocity of traveltime that follows from the assumption of non-converted reflection rays. It is assumed that the midpoint displacement, Δm and half-offset, h, are small quantities.

These parameters carrie informations that can be related to geophysical attributes (see Equation 3. The parameter a is the slope of the traveltime curve at (m_0, t_0). It contains information about the emergence angle, β, of the reference (normal) ray, with respect to the normal as well as the local near-surface velocity, v_0, at the point m_0 at the measurement surface. The parameter C is related to the curvature, K_{NIP}, of a hypothetical wavefront measured at the reference point m_0 and associated with a point source located at the point of incidence of the normal ray. Also, parameter C can be related to the NMO-velocity. The parameter B is related to the curvature, K_N, of another hypothetical wavefront that originates from a region in the vicinity of the same normal incidence point as an exploding reflector. For more detailed information on these quantities, the reader is referred to (see, e.g., Jäger et al., 2001). We have

$$a = \frac{2\sin\beta}{v_0} \,, \quad B = \frac{2t_0\cos^2\beta}{v_0}K_N \quad \text{and} \quad C = \frac{2t_0\cos^2\beta}{v_0}K_{NIP} = \frac{4}{v_{NMO}^2}. \tag{3}$$

SURGICAL CRS WORKFLOW

Figure 1 summarizes the proposed workflow and assigns a number for each processing step. In the following, these steps will be discussed in detail.

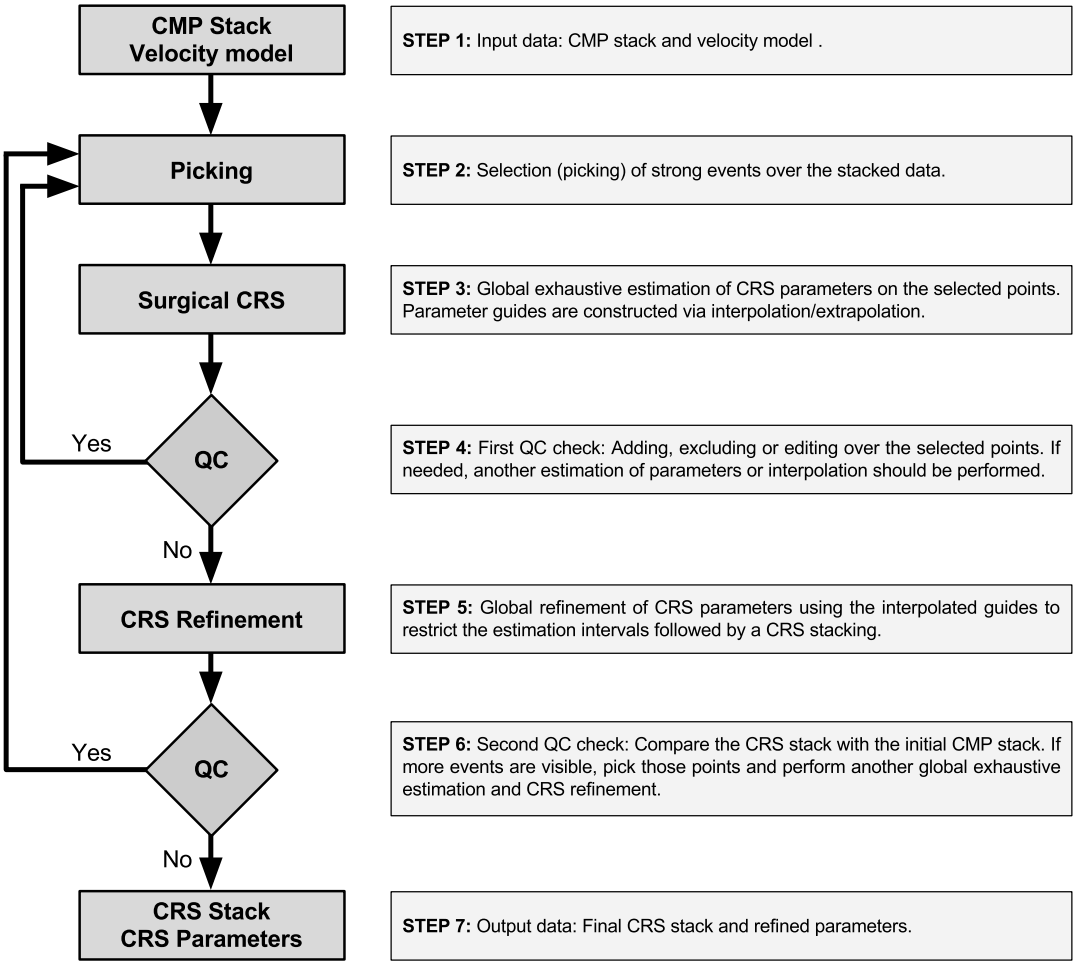

Figure 1: Workflow for CRS stacking using the proposed approach alongside with a brief description of each processing step.

- **STEP 1**: A conventional CMP stacked data and its corresponding NMO-velocity model are needed as input. In this case, both can be considered given, since they are part of conventional routine sequence of seismic processing.
- **STEP 2**: Select (pick) points along key events on the CMP stacked section. These picks should follow only the stronger events, avoiding all regions where these events are not well focused or with low signal-to-noise ratio. The objective is to ensure that only well-defined regions will contribute to the construction of the parameter guides. Note that, even in cases where only a very small portion of the dataset is well focused, which leads to a small number of picks, this approach is able yield good results after a number of iterations.
- **STEP 3**: For each selected point, or pick, a global exhaustive estimation of CRS parameters will be performed using the initial NMO-velocity model as a guide. This estimation process computes the coherence for all possible 3-uplets (2D case) or 8-uplets (3D case) within a chosen search interval. After that, the set of CRS parameters with maximum coherence is selected.

Remark: It is worth mentioning that, this approach is prohibitive to be performed over to entire dataset. However, since the (surgical) set of selected points constitutes a very small fraction of the data, it can be very cheaply computed.

Once the CRS parameters are estimated at each (surgically) selected point, interpolation and extrapolation schemes are employed to fill out all parameter-section grids and construct the parameter guides.

- **STEP 4**: In order to avoid guides with non-geological information a Quality Control (QC) procedure is considered. Although the picking was done only on well-focused events in the CMP stack, some picks may be interpreted as parameter outliers which compromises the guide. A visual comparison between the obtained guides and the CMP stacked data is enough to find such inconsistencies.

  If needed, new points can be picked, excluded or edited. In this case, another estimation and/or interpolation/extrapolation is to be performed.

- **STEP 5**: A global refinement is performed considering small deviations of the guides for every time sample and midpoint position. Once again, the coherence maximum is selected, the refined guides are stored and the dataset is stacked.

  Remark: Since we are assuming that the optimized, estimated-for parameter is close to its actual value, the amount of estimations needed for each sample is significantly reduced. Also, the estimation interval (deviations) for each CRS parameter should diminish as more iterations are conducted. This means that each iteration is cheaper than the previous one.

- **STEP 6**: Now, a new QC procedure is considered, where the CMP (input data) and the CRS stacked data (obtained in the previous step) are compared. Experiments showed that after the first iteration, the CRS stack presented better defined events and also new events become visible. In this case, a new iteration is to be done, considering picks along the new events and (if needed) correcting some of the previous picks.

- **STEP 7**: After a number of iterations, the final CRS stack and parameters are obtained. A criterion for that is that changes in the last iteration become un-noticeable.

APPLICATION

For a given 2D dataset, surgical CRS is now applied and compared with the corresponding results of conventional CMP and data-driven CRS. The dataset consists of a land seismic line of the Tacutu basin in the Brazilian northern region, close to the border with Guyana. Acquired in 1985, the dataset has a 4 ms time sampling interval, 12.5 m between CMP gathers with maximum fold of 12 traces. Due to the small fold and poor signal-to-noise ratio, the Tacutu dataset is a good candidate for applying the CRS method, since that method makes full use of the available data redundancy. The half-offset and midpoint apertures were the same as the ones considered in Faccipieri et al. (2015). This means that the apertures in midpoints are small enough so that midpoint curvature (parameter B) can be assumed as very close to zero). Also, in both CRS results, global estimation of parameters has been employed.

Figure 2 (a) shows a CMP stack obtained using a conventional velocity analysis was performed by an interpreter; Figure 2 (b) shows CRS stack, obtained selecting proper estimation intervals for the CRS parameters; Figure 2 (c) presents the Surgical CRS stack, obtained using parameter guides (velocity and emergence angles) after two iterations. Note that the Conventional CRS stacking was able to enhance the events observable on the CMP stack and also give rise to several new events. A similar increase in quality can be observed comparing the Conventional CRS with the proposed Surgical CRS stack. However, this comparison can be greatly facilited if we consider only small target region of the dataset.

Target region Figures 3 shows in detail the previous results for the upper left region of the data. As discussed above, the main events (and also part of the weaker) present on the CMP stack were enhanced by the CRS method. However, the Surgical CRS stack was able to stack coherently more events, especially on the middle region. This difference can be explained by the estimation strategies involved on each approach.

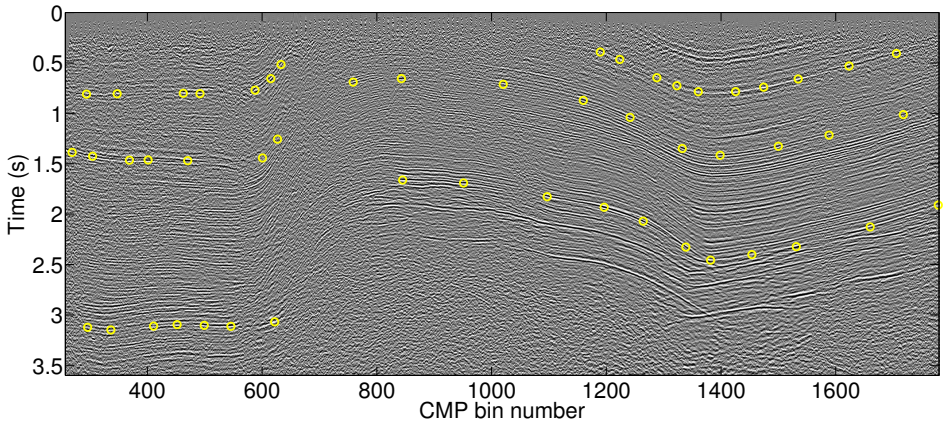

(a) CMP stacked section.

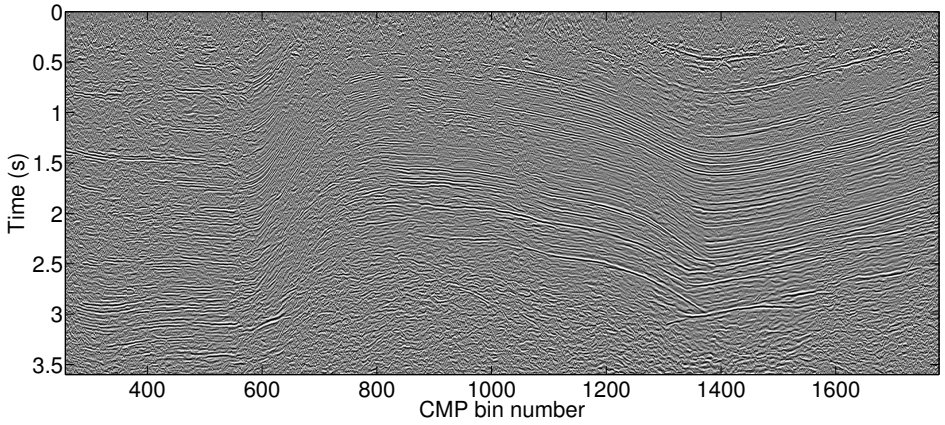

(b) CRS stacked section.

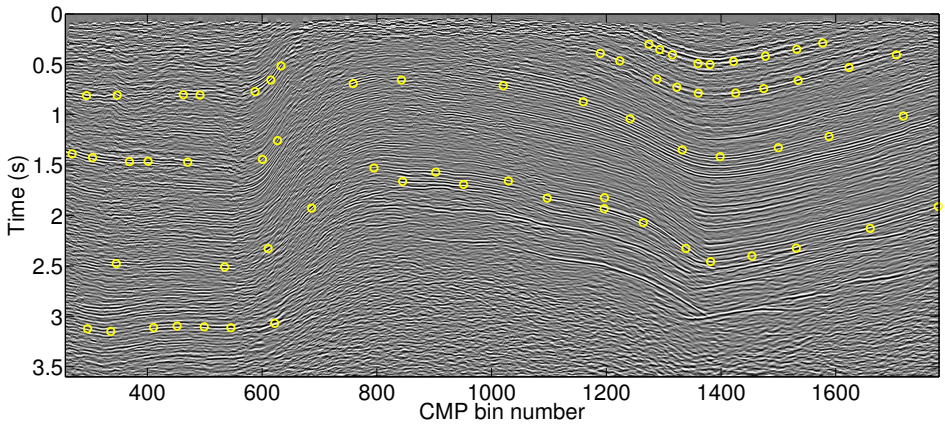

(c) Surgical CRS stacked section (Second iteration).

Figure 2: Comparison among CMP, CRS and Surgical CRS stacked sections. The yellow circles represent the selected points, where the parameters were computed using a global exhaustive estimation.

The data-driven approach used to obtain the CRS stack may be compromised by noise and coherent events, generating artifacts (e.g., so-called CRS worms). In the case of Surgical CRS, guides preserve the expected geological tendency of the CRS parameters, avoiding these inconsistencies.

On the first iteration of Surgical CRS, the parameter guide was constructed based on points selected (picked) on the CMP stack. These picks are represent by yellow circles over the stacked section and can be seen on Figures 3 (a). For them, a global exhaustive estimation of CRS parameters was performed using an initial velocity model (see Figure 4 (a)) to stabilize the estimation. The estimated emergence angles and curvatures were interpolated generating the guides showed on Figures 4 (c) and 4 (e).

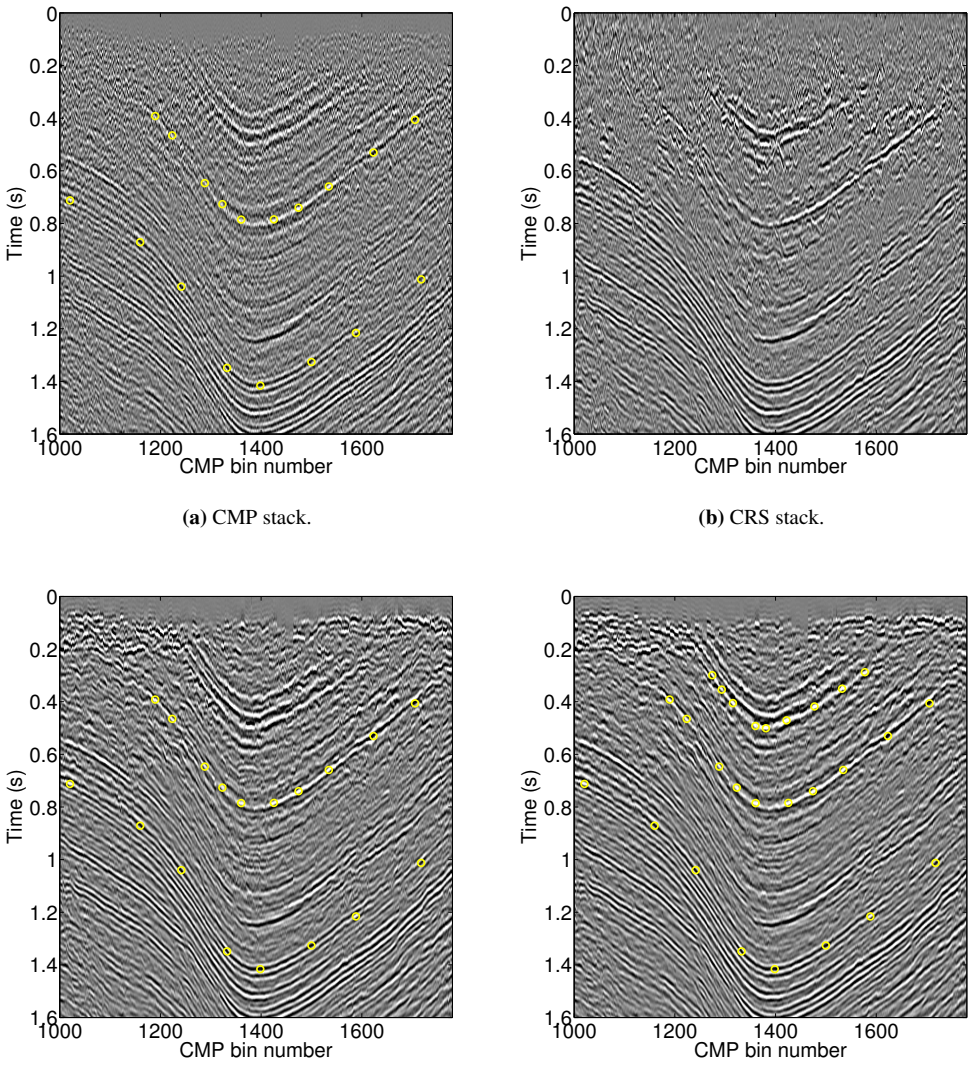

(a) CMP stack.

(b) CRS stack.

(c) Surgical CRS stack (First iteration).

(d) Surgical CRS stack (Second iteration).

Figure 3: Target Region: Comparison among CMP, CRS and Surgical CRS stacked sections. The yellow circles represent the selected points used to construct the first and second emergence angle guides.

Now, a CRS refinement is performed over all time samples and midpoints using the velocity, the emergence angle and curvature guides (Figures 4 (a), 4 (c) and 4 (e), respectivelly). The allowed deviation from the guides for velocity, emergence angles and curvatures was 10%, $\pm 5°$and 20%, respectively. The obtained stacked section (firs iteration of Surgical CRS) and the refined guides can be seen on Figure 3 (c) and Figures 5 (a), 5 (c) and 5 (e).

After the first iteration, one can observe that the resulting stacked section of Surgical CRS is much clear than the CMP stacked section. Following the proposed workflow, new points were selected on the enhanced stacked section and a second iteration was performed. Figures 4 (b), 4 (d) and 4 (f) shows the parameter guides, for velocity, emergence angles and curvatures, obtained interpolating the values estimated on the Surgical CRS (Global exhaustive estimation). These guides were refined allowing a smaller deviation for velocity and emergence angles (5%, $\pm 2°$and 10%, respectively) and can be found on Figures 5 (b), 5 (d) and 5 (f). Stacking the dataset with these refined guides, we obtain the second iteration of Surgical CRS (see Figure 3 (d)). For comparison, the velocity, emergence angles and curvatures obtained with the data-driven CRS can be found on Figure 6. Note that, along strong events, they match almost perfectly with the guides. However, where the events are weaker the parameters tend to deviates from the geological tendency.

Regarding computational effort, Table 1 compares the costs involved in Surgical and data-driven CRS for our illustrative dataset. For that comparison, we used the number of semblance evaluations as our cost unit. In the case of data-driven CRS, a total of 5.177×10^9 semblances were computed against 1.509×10^9 semblances for the Surgical CRS (summing the two iterations), which leads to an acceleration of almost 3.5 times.

Table 1: Computational cost (in number of Semblances) for CRS and Surgical CRS.

		# Semblances per sample	# samples	Total ($\times 10^9$)
	CRS	3150	1643520	5.177
Iteration 1	Surgical CRS	4000000	52	0.208
	CRS Refinement	375	1643520	0.616
	Total	–	–	0.824
Iteration 2	Surgical CRS	4000000	17	0.068
	CRS Refinement	375	1643520	0.616
	Total	–	–	0.684
Iteration 1 + 2	Total	–	–	1.509

CONCLUSIONS

O novel workflow for implementation of the Common-Reflection-Surface (CRS) method has been introduced. The workflow is an iterative process, in which, in each iteration (a) the estimation of CRS parameters is restricted to a few, carefully (or surgically) selected points. Away from these points, CRS parameter values are obtained from interpolation/extrapolation procedures and (b) Surgical points are selected by manual picking, conveying, in this way, valuable geological content. Because full parameter estimations (the most expensive part in any CRS algorithm) is restricted to a restricted (surgical) selection of points, the proposed approach achieves substantial savings in computation effort. A possible tradeoff is the requirement of human interference (manual picking) in the selection of those points.

For illustrative purposes, (two-iteration) Surgical CRS has been applied to a real 2D land seismic dataset and compared corresponding applications of conventional CMP and full-parameter estimation CRS. The results were plainly favorable to the proposed approach. Besides extension to 3D, present studies are devoted to algorithmic issues, such as interpolation/extrapolation routines and more transparent criteria for the choice of surgical points.

ACKNOWLEDGMENTS

J. Faccipieri, D. Rueda, T. Coimbra, I. Rodrigues, A. L. Farias and M. Tygel acknowledge support from the National Council for Scientific and Technological Development (CNPq-Brazil), the National Institute of Science and Technology of Petroleum Geophysics (ICTP-GP-Brazil), the Center for Computational Engineering and Sciences (Fapesp/Cepid # 2013/08293-7-Brazil) and the Brazilian Oil Company - Petrobras (Cooperation term # 0050.0066919.11.9). The authors finally acknowledge support of the sponsors of the Wave Inversion Technology (WIT) Consortium.

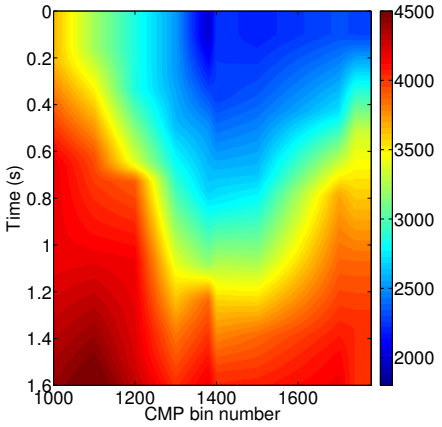

(a) First iteration: Velocity guide in m/s.

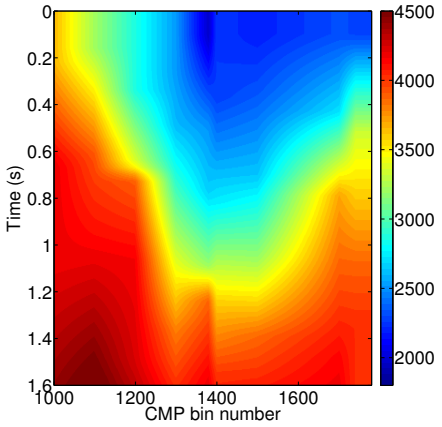

(b) Second iteration: Velocity guide in m/s.

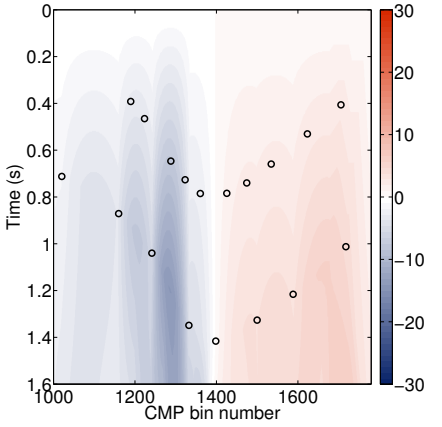

(c) First iteration: Emergence angle guide in degrees.

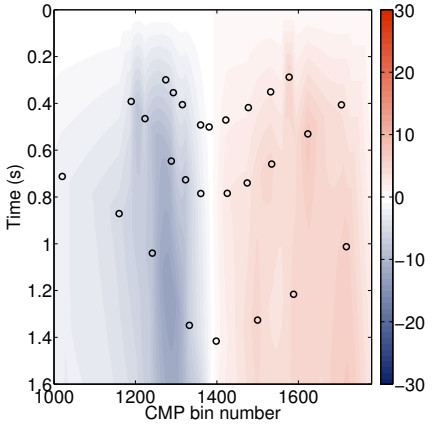

(d) Second iteration: Emergence angle guide in degrees.

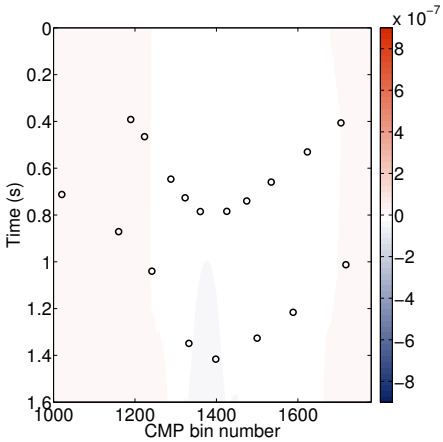

(e) First iteration: Curvature guide in s^2/m^2.

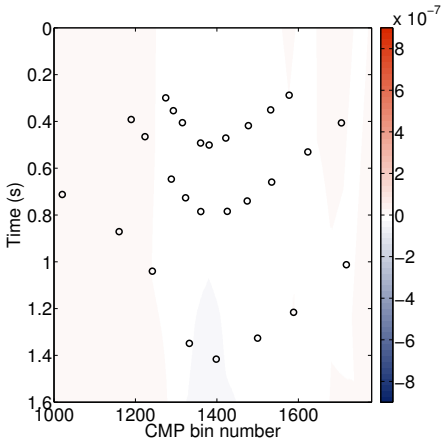

(f) Second iteration: Curvature guide in s^2/m^2.

Figure 4: Target Region: Parameter guides for velocity, emergence angles and curvatures used on the first and second iteration of Surgical CRS. The black circles represent the selected points, where the parameters were computed using a global exhaustive estimation. All other values were constructed thought interpolation/extrapolation schemes.

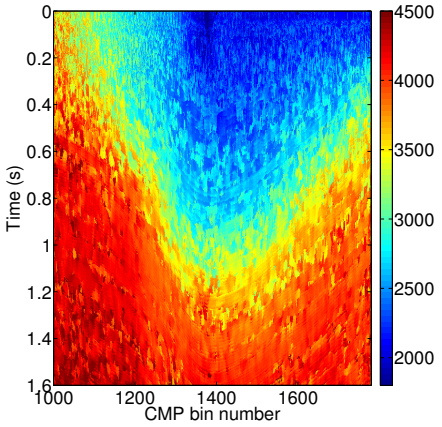

(a) First iteration: Refined velocity guide in m/s.

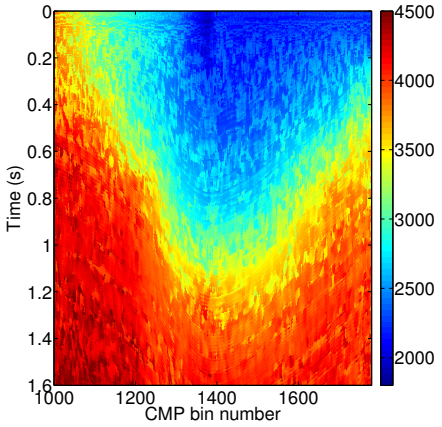

(b) Second iteration: Refined velocity guide in m/s.

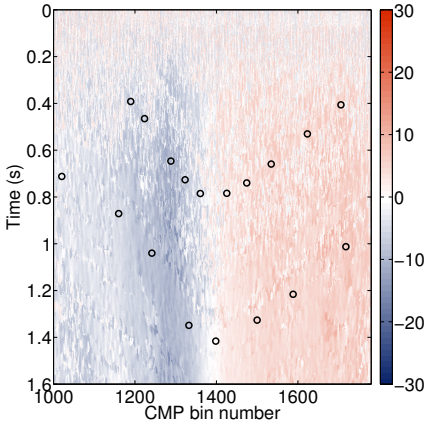

(c) First iteration: Refined emergence angle guide in degrees.

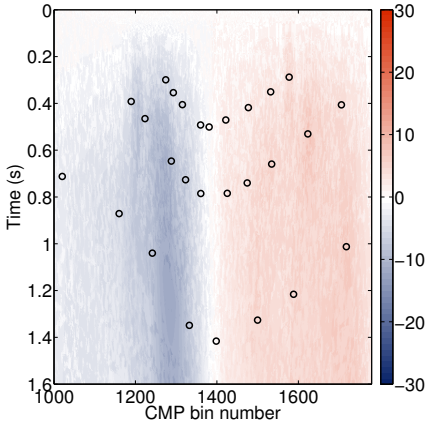

(d) Second iteration: Refined emergence angle guide in degrees.

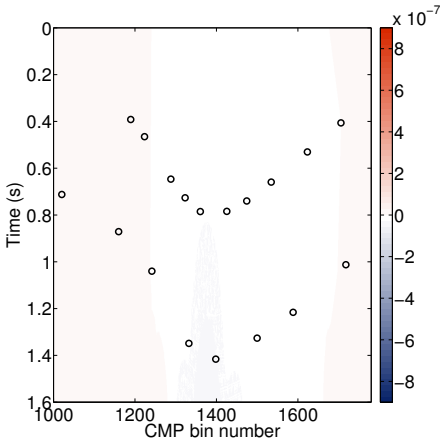

(e) First iteration: Refined curvature guide in s^2/m^2.

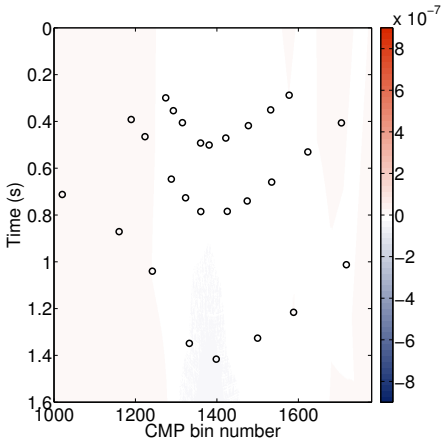

(f) Second iteration: Refined curvature guide in s^2/m^2.

Figure 5: Target Region: Refined parameter guides for velocity, emergence angles and curvatures obtained after the first and second iteration of Surgical CRS. The black circles represent the selected points, where the parameters were computed using a global exhaustive estimation. All other values were refined by the CRS method.

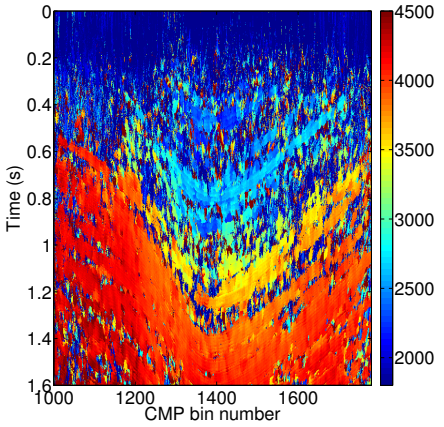

(a) CRS estimated velocities in m/s.

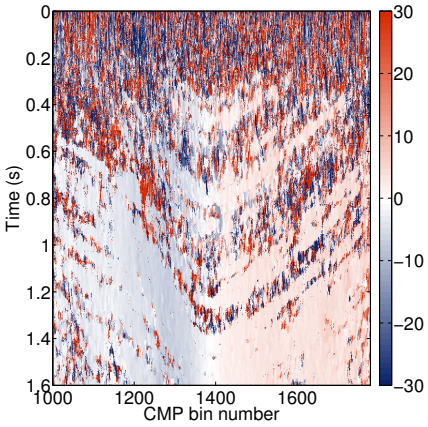

(b) CRS estimated emergence angles in degrees.

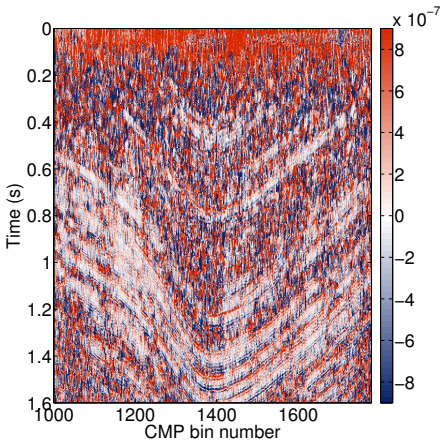

(c) CRS estimated curvature in s^2/m^2.

Figure 6: Velocity, emergence angles and curvatures estimated by the CRS method without using guides. The estimation intervals for each parameter were restricted to values present on the data.

REFERENCES

Bergler, S., Hubral, P., Marchetti, P., Cristini, A, M., and Cardone, G. (2002). 3D common-reflection-surface stack and kinematic wavefield attributes. *The Leading Edge*, 21(10):1010–1015.

Berkovitch, A., Belfer, I., and Landa, E. (2008). Multifocusing as a method of improving subsurface imaging. *The Leading Edge*, 2:250–256.

Dell, S., D. G. and Vanelle, C. (2012). Prestack time migration by common-migrated-reflector-element stacking. *Geophysics*, 77(3):S73–S82.

Dell, S., Gajewski, D., and Tygel, M. (2014). Image ray tomography. *Geophysical Prospecting*, 62(3):413–426.

Duveneck, E. (2004). 3D tomographic velocity model estimation with kinematic wavefield attributes. *Geophysical Prospecting*, 52(6):535–545.

Faccipieri, J., Coimbra, T., Gelius, L.-J., and Tygel, M. (2015). *Bi-parametric traveltimes and stacking apertures for reflection and diffraction enhancement*, pages 1355–1360. 14th International Congress of the Brazilian Geophysical Society. SBGf, Expanded Abstracts.

Faccipieri, J., Serrano, D., Gelius, L.-J., and Tygel, M. (2013). Recovering diffractions in crs stacked sections. *First Break*, 31:27–31.

Fomel, S. and Kazinnik, R. (2013). Non-hyperbolic common reflection surface. *Geophysical Prospecting*, 61(1):21Ű27.

Garabito, G., Cruz, J. C., Hubral, P., and Costa, J. (2001). Common reflection surface stack: A new parameter search strategy by global optimization. In *SEG, Expanded Abstracts*, pages 2009–2012.

Garabito, G., Stoffa, P. L., Lucena, and Söllner, W. (2013). *Global optimization of the common-offset CRS-attributes: Synthetic and field data application*, pages 1565–1568. 13th International Congress of the Brazilian Geophysical Society & EXPOGEF. SBGf, Expanded Abstracts.

Gelchinsky, B., Berkovitch, B., and Keydar, S. (1999a). Multifocusing homeomorphic imaging - Part 1. *Journal of Applied Geophysics*, 42:229–242.

Gelchinsky, B., Berkovitch, B., and Keydar, S. (1999b). Multifocusing homeomorphic imaging - Part 2. *Journal of Applied Geophysics*, 42:243–260.

Gelius, L.-J. and Tygel, M. (2015). Migration-velocity building in time and depth from 3D (2D) common-reflection-surface (CRS) stacking - theoretical framework. *Studia Geophysica et Geodaetica*, 59:253–282.

Hertweck, T., Schleicher, J., and Mann, J. (2007). Data stacking beyond cmp. *The Leading Edge*, 26(7):818–827.

Jäger, R., Mann, J., Höcht, G., and Hubral, P. (2001). Common-reflection-surface stack: Image and attributes. *Geophysics*, 66(1):97–109.

Landa, E., Gurevich, B., Keydar, S., and Trachtman, P. (1999). Application of multifocusing method for subsurface imaging. *Journal of Applied Geophysics*, 42:283–300.

Landa, E., Keydar, S., and Moser, T. J. (2010). Multifocusing revisited - inhomogeneous media and curved interfaces. *Geophysical Prospecting*, 58:925–938.

Müller, T., Jäger, R., and Höcht, G. (1997). Common reflection surface staking method - imaging with an unknown velocity model. *68th Annual Internat. Mtg., Soc. Expl. Geophys.*, pages 1770–1773.

Perroud, H., Krummenauer, R., Tygel, M., and Lopes, R. R. (2014). Parameter estimation from non-hyperbolic reflection traveltimes for large aperture common midpoint gathers. *Near Surface Geophysics*, 12:679–686.

Schwarz, B., Vanelle, C., Gajewski, D., and Kashtan, B. (2014). Curvatures and inhomogeneities: an improved common-reflection-surface approach. *Geophysics*, 79(5):S231–S240.

Spinner, M. and Mann, J. (2005). *True-amplitude CRS-based Kirchhoff time migration for AVO analysis*, pages 246–249. SEG Mtg. SEG, Expanded Abstracts.